Biochimica et Biophysica Acta 1838 (2014) 1019–1030

Contents lists available at ScienceDirect

Biochimica et Biophysica Acta

journal homepage: www.elsevier.com/locate/bbamem

Investigating the interactions of the 18 kDa translocator protein and its ligand PK11195 in planar lipid bilayers

Claire R. Hatty [a], Anton P. Le Brun [b], Vanessa Lake [b], Luke A. Clifton [c], Guo Jun Liu [a,d], Michael James [b,e,1], Richard B. Banati [a,d,*]

[a] Medical Imaging & Radiation Sciences Faculty Research Group, Faculty of Health Sciences, The University of Sydney, c/o Brain & Mind Research Institute, 94 Mallett Street, Camperdown, NSW 2050, Australia
[b] Bragg Institute, Australian Nuclear Science and Technology Organisation, New Illawarra Road, Lucas Heights, NSW 2234, Australia
[c] ISIS Pulsed Neutron and Muon Source, Science and Technology Facilities Council, Rutherford Appleton Laboratory, Harwell Oxford, Didcot OX11 0QX, UK
[d] Life Sciences, Australian Nuclear Science and Technology Organisation, New Illawarra Road, Lucas Heights, NSW 2234, Australia
[e] School of Chemistry, University of New South Wales, Kensington NSW 2052, Australia

ARTICLE INFO

Article history:
Received 17 October 2013
Received in revised form 16 December 2013
Accepted 18 December 2013
Available online 27 December 2013

Keywords:
TSPO
PK11195
QCM-D
Neutron reflectometry
Membrane protein
Lipid bilayer

ABSTRACT

The functional effects of a drug ligand may be due not only to an interaction with its membrane protein target, but also with the surrounding lipid membrane. We have investigated the interaction of a drug ligand, PK11195, with its primary protein target, the integral membrane 18 kDa translocator protein (TSPO), and model membranes using Langmuir monolayers, quartz crystal microbalance with dissipation monitoring (QCM-D) and neutron reflectometry (NR). We found that PK11195 is incorporated into lipid monolayers and lipid bilayers, causing a decrease in lipid area/molecule and an increase in lipid bilayer rigidity. NR revealed that PK11195 is incorporated into the lipid chain region at a volume fraction of ~10%. We reconstituted isolated mouse TSPO into a lipid bilayer and studied its interaction with PK11195 using QCM-D, which revealed a larger than expected frequency response and indicated a possible conformational change of the protein. NR measurements revealed a TSPO surface coverage of 23% when immobilised to a modified surface via its polyhistidine tag, and a thickness of 51 Å for the TSPO layer. These techniques allowed us to probe both the interaction of TSPO with PK11195, and PK11195 with model membranes. It is possible that previously reported TSPO-independent effects of PK11195 are due to incorporation into the lipid bilayer and alteration of its physical properties. There are also implications for the variable binding profiles observed for TSPO ligands, as drug–membrane interactions may contribute to the apparent affinity of TSPO ligands.

1. Introduction

Integral membrane proteins are the binding targets of a wide range of pharmaceutical compounds due to their role in vital cellular functions, such as transport of molecules across biological membranes. The 18 kDa translocator protein (TSPO), a protein located primarily in the outer mitochondrial membrane, is a particularly attractive target in the development of therapeutic drugs. It is implicated in a variety of functions including apoptosis, steroidogenesis and immunomodulation [1,2], and TSPO ligands have shown promise in the treatment of conditions including anxiety [3], some cancers [2], neuroinflammation and neurodegeneration [4,5]. TSPO and its synthetic ligands are also of diagnostic value for in vivo imaging, as TSPO expression is up-regulated during neuroinflammation and in some types of cancer, which makes it a valuable target for visualising the progression of these conditions [6,7].

An understanding of the structure of TSPO provides valuable insight into its function and interaction with ligands, knowledge that is essential in the development of pharmacological interventions that target TSPO. In particular, changes in conformation due to ligand binding and the implication for functions such as transport need to be understood at the molecular level. As an integral membrane protein TSPO presents a challenge for structural investigations, and there is limited experimental data on TSPO structure. The current model of TSPO describes it as an integral membrane protein consisting of five transmembrane alpha helices [8], an extramitochondrial C-terminal containing a cholesterol

Abbreviations: ANTA, nitrilotriacetic acid group with a terminal amino group; Bmax, maximal number of receptor binding sites; CMAu, gold contrast matched water; CMSi, silicon contrast matched water; CM4, scattering length density 4 contrast matched water; DDM, n-dodecyl-β-D-maltopyranoside; DMPC, 1,2-dimyristoyl-sn-glycero-3-phosphocholine; DMPE, 1,2-dimyristoyl-sn-glycero-3-phosphoethanolamine; DTSP, dithiobis(succinimidyl propionate); DTT, dithiothreitol; *E. coli*, *Escherichia coli*; IPTG, isopropyl β-D-1-thiogalactopyranoside; Kd, affinity or equilibrium dissociation constant; NR, neutron reflectometry; NSAIDs, non-steroidal anti-inflammatory drugs; NTA, nitrilotriacetic acid; OD, optical density; PBS, phosphate buffered saline; PC, phosphatidylcholine; PK11195, 1-(2-Chlorophenyl)-N-methyl-N-(1-methylpropyl)-3-isoquinolinecarboxamide; QCM-D, quartz crystal microbalance with dissipation monitoring; SDS, sodium dodecyl sulphate; SLD, scattering length density; SPR, surface plasmon resonance; SUV, small unilamellar vesicle; TEV, tobacco etch virus; TSPO, translocator protein; TspO, tryptophan rich sensory protein

* Corresponding author at: Life Sciences, Australian Nuclear Science and Technology Organisation, New Illawarra Road, Lucas Heights, NSW 2234, Australia. Tel.: +61 2 9717 3505.
E-mail address: rib@ansto.gov.au (R.B. Banati).
[1] Current address: Australian Synchrotron, 800 Blackburn Road, Clayton, VIC 3168, Australia.

0005-2736/$ – see front matter © 2013 Published by Elsevier B.V.
http://dx.doi.org/10.1016/j.bbamem.2013.12.013

binding domain [9], an intramitochondrial N-terminal, two extramitochondrial loops and two intramitochondrial loops [10], forming a channel that transports cholesterol across the membrane [11].

The structure and activity of a membrane protein is modulated not only by direct interaction with its ligands, but is also influenced by the lipid membrane environment in which it resides. There is increasing recognition that the lipid membrane is more than an inert scaffold for proteins, and that the arrangement of lipids in membranes carries functional significance for drug interactions. There is evidence that certain drugs, for example some NSAIDs and anaesthetics, may modulate function by inducing physical changes in the membrane environment, thereby affecting the conformation and function of proteins within the membrane [12,13]. Thus, the observed effect of a drug may not be due solely to receptor–ligand binding, but the interplay between both drug–membrane and drug–protein interactions. In developing pharmacological interventions we need an understanding of how drugs interact both with their membrane protein targets and the surrounding membrane environment.

PK11195 is an isoquinoline carboxamide derivative (Fig. 1) and nanomolar affinity ligand for TSPO which has been used extensively for imaging studies and investigating TSPO function. However, it has also been shown to have functional effects that are independent of interaction with TSPO, typically at micromolar concentrations, well above the Kd for TSPO. There is evidence that PK11195 can sensitise cancer cells to apoptosis and to the effects of other chemotherapeutics via a TSPO-independent mechanism [14–17]. The exact mechanism is unclear, but in some instances PK11195 appears to modulate drug efflux activity to overcome multiple drug resistance [16,17]. Given the high lipophilicity of PK11195, and previous evidence that it affects the lipid fluidity of mitochondria [18], the ability of other compounds to chemosensitise [19], activate apoptosis [20], and inhibit proliferation of cancer cells by interacting with lipid membranes to change their physical properties [21,22], it is possible that this is one mechanism through which PK11195 induces TSPO-independent effects at high concentration.

There is growing interest in studying the structure and function of membrane proteins in a more natural membrane environment. It is possible to study the function of membrane proteins reconstituted into planar lipid bilayers using surface sensitive techniques such as quartz crystal microbalance with dissipation monitoring (QCM-D), surface plasmon resonance (SPR), and electrical impedance spectrometry (EIS) [23]. Furthermore, the structure of planar protein/lipid bilayers can be studied using neutron reflectometry (NR) [24,25]. Techniques to form these protein/lipid bilayers have included covalently linking an engineered protein to the surface and reconstituting lipid around it, or inserting the protein into a pre-formed lipid bilayer [24,25]. Proteins with a polyhistidine tag can be reversibly immobilised to a gold surface that has been functionalised to a nickel or copper chelating nitrilotriacetic acid (NTA) surface, and a lipid bilayer reconstituted around the detergent solubilised membrane protein by replacing detergent molecules with lipid [23,26]. Studies using surface tethered protein have shown that functions such as electron transport [26] and ligand binding [27–29] remain intact with protein immobilisation.

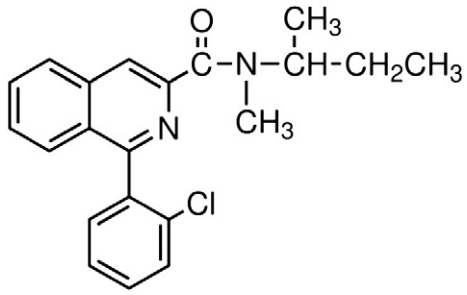

Fig. 1. The TSPO ligand PK11195.

TSPO has been studied in model membrane environments such as detergent micelles for investigating tertiary structure with NMR [8], liposomes for structural investigation with electron microscopy [30], and more recently in lipid bilayers for investigating oligomerisation with electron microscopy [31]. TSPO has not been studied in planar membranes using QCM-D or NR. QCM-D provides information about the mass, rigidity and thickness of biomimetic membranes, and can be used to sense ligand interactions and protein conformational changes. NR allows us to study the thickness and composition of planar model membranes in an aqueous environment, and with the use of isotopic contrast the lipid, protein and ligand components can be selectively highlighted. This work was aimed at better understanding the interaction of a TSPO drug ligand, PK11195, with both the TSPO and the surrounding lipid membrane environment using QCM-D and NR.

2. Materials and methods

2.1. Materials

Chemicals and reagents were purchased from Sigma-Aldrich (Sydney, New South Wales, Australia) unless otherwise stated. Lipids and cholesterol were purchased from Avanti Polar Lipids (Alabaster, Alabama, USA). Silicon substrates for neutron reflectometry were purchased from Crystran (Poole, Dorset, UK). Silicon substrates for SURF neutron reflectometry experiments were coated with chromium and gold at the NIST NanoFab facility (National Institute of Standards and Technology, Gaithersburg, MD, USA). Quartz crystals coated with SiO_2 or gold were purchased from Q-Sense (Stockholm, Sweden).

2.2. TSPO expression and purification

Cells of the BL21(DE3) *Escherichia coli* strain (Invitrogen/Life Technologies, Mulgrave, VIC, Australia) were transformed with the pET(TEV) 28aTSPOm vector, which produces full-length recombinant mouse TSPO protein with an N-terminal 6xHis-tag joined by a TEV cleavage site. The cells were grown in Fernbach flasks in ModC1 media [32] containing 40 μg/ml kanamycin in a shaking incubator at 37 °C at 220 rpm to an OD_{600} of ~0.6 before the expression of TSPO was induced by the addition of 1 mM isopropyl β-D-1-thiogalactopyranoside (IPTG). Cells were grown for a further 5 h after induction, and then harvested by centrifugation at 8000 × *g* for 30 min at 4 °C.

The cell pellet was then resuspended in lysis buffer (50 mM HEPES, 150 mM NaCl, 1 mM DTT, 1 mM EDTA, pH 7.8) with the addition of 1 mg/ml lysozyme and 5 μg/ml DNAase I. The cells were lysed by sonicating on ice for 6 × 30 s bursts at 40 W with an ultrasonic probe. The lysate was centrifuged at 15,000 rpm in a Beckman JA 25.5 rotor at 4 °C for 20 min to pellet the insoluble inclusion bodies. Inclusion bodies were then washed 3 times by resuspending in lysis buffer containing 1% Triton X-100 and centrifuging at 15,000 rpm for 20 min. The final pellet of inclusion bodies was solubilised in binding buffer (50 mM HEPES, 150 mM NaCl, 5 mM imidazole, 1% SDS (wt/vol), pH 7.8), before finally centrifuging at 15,000 rpm for 30 min at 20 °C. Solubilised inclusion bodies were applied to a Qiagen Superflow Ni-NTA gravity flow column (Qiagen, Chadstone, VIC, Australia), washed with buffer containing 10 mM imidazole, and TSPO was eluted with 250 mM imidazole in 1% SDS.

2.3. Preparation of liposomes and proteoliposomes

Lipid vesicles for use in QCM-D and neutron reflectometry were prepared as follows. Stock solutions of DMPC (20 mg/ml in chloroform), DMPE (5 mg/ml in 3:1 chloroform/methanol), cholesterol (20 mg/ml in chloroform) or PK11195 (20 mg/ml in chloroform) were mixed according to the desired composition, and the solvent was evaporated under nitrogen to form a dry lipid film. The lipids were resuspended in Tris buffer (10 mM Tris–HCl, 150 mM NaCl, pH 7.4) to a concentration

of 1 mg/ml, hydrated for 2 h at 45–55 °C, and finally sonicated to produce small unilamellar vesicles (SUVs). The suspension of SUVs was then kept at 45 °C for use on the same day. The 1 mg/ml suspension was diluted to 0.05 mg/ml with Tris buffer for use in QCM-D. Proteoliposomes composed of DMPC/DMPE (9:1) and TSPO in a 4:1 (wt/wt) ratio were prepared using a method previously described [30].

2.4. Radioligand binding

Proteoliposomes (1 μg) were incubated in a final volume of 500 μl of 50 mM Tris–HCl (pH 7.4) with 0.6 nM–10 nM tritium labelled PK11195 (^{3}H-PK11195) in the absence or presence of 10 μM unlabelled PK11195. Samples were incubated in triplicate for 90 min at 0 °C. The incubation was terminated by vacuum filtration over Whatman GF/C filters, followed by 4 washes with ice-cold Tris buffer. Liposomes (1 μg) without protein were incubated under the same conditions in parallel as a control. Radioactivity trapped on the filters was measured by liquid scintillation counting. Saturation binding data were analysed using GraphPad Prism 5 (GraphPad Software, La Jolla, California, USA) to fit Bmax and Kd.

2.5. Langmuir monolayers

Monolayers were formed on the surface of phosphate buffered saline (PBS) in a Langmuir trough (Nima Technology, Coventry, UK) with a Wilhelmy plate made from Whatman Chr1 chromatography paper. DMPC, PK11195 or DMPC/PK11195 monolayers were formed by depositing 40 μl of a 0.2 mg/ml chloroform solution across the subphase surface. After all solvent had been allowed to evaporate, the barriers were closed gradually to compress the monolayer while measuring the pressure-area isotherm. The surface pressure vs. molecular area for each monolayer was recorded by the Nima software (Nima Technology, Coventry, UK), exported and plotted in GraphPad Prism 5.

2.6. QCM-D

The Q-Sense E4 quartz crystal microbalance with dissipation monitoring (QCM-D) (Q-Sense, Sweden) was used for all QCM-D measurements. SiO_2 coated sensor crystals were cleaned by UV ozone for 15 min, followed by soaking in 2% Hellmanex solution for 10–30 min, rinsed thoroughly with ultrapure water, dried, and finally UV cleaned for a further 10 min. Once the sensors had been placed in the measurement chamber they were further rinsed with ultrapure water, spectrophotometric grade ethanol, and finally ultrapure water. Planar lipid bilayers were formed on the SiO_2 surface of sensor crystals using the method of vesicle adsorption and rupture described in the literature [33,34]. Experiments were performed at 37 °C in Tris buffer (10 mM Tris–HCl, 150 mM NaCl, pH 7.4). A 0.05 mg/ml suspension of SUVs was injected into each chamber at 100 μl/min, and vesicles were allowed to incubate on the surface for up to 30 min before excess vesicles were rinsed away resulting in the formation of a planar lipid bilayer.

Gold coated sensor crystals were used for the formation of TSPO/lipid bilayers. Gold surfaces were cleaned by exposing the surface to a solution of $H_2O_2/NH_3/H_2O$ (1:1:5) at 70 °C for 10 min, then rinsing with ultrapure water and ethanol. The gold surface of the sensor crystal was then modified with DTSP-ANTA-Cu^{2+} according to the method of Giess et al. [23] in order to allow the selective binding of His-tagged proteins to the surface. His-tagged mouse TSPO was immobilised to the sensor surface in situ while the process was monitored in real time using the change in frequency (Δf) and dissipation (ΔD) measurements of the QCM-D. Buffer containing 0.5% SDS (wt/vol) was injected and allowed to stabilise for approximately 10 min, followed by 900 μl of 50 μg/ml TSPO solution containing 0.5% SDS (wt/vol) at a flow rate of 100 μl/min. The protein solution was left to incubate on the surface for 30–60 min, before being rinsed with buffer containing 0.5% SDS (wt/vol). A DMPC/DMPE (9:1) bilayer was formed around the immobilised TSPO by gradually replacing the detergent surrounding the protein with lipid. First, a solution of mixed lipid–detergent vesicles containing 0.05 mg/ml lipid and 0.035% SDS (wt/vol) was injected into the chamber and allowed to incubate on the surface for 30 min. A solution of lipid only vesicles at 0.05 mg/ml was then injected and allowed to incubate on the surface for 60 min in order to allow lipid molecules to be incorporated into a bilayer around the protein and to replace detergent molecules. This method was adapted from Giess et al. [23] and Vacklin et al. [35]. After lipid vesicles had been incubated with the protein, excess vesicles were rinsed off with Tris buffer to complete protein/lipid bilayer formation.

The interaction of lipid only and TSPO/lipid bilayers with the TSPO ligand PK11195 was investigated by injecting a solution of 100 μM PK11195 in Tris buffer over the bilayers and allowing it to incubate for 90 min. Before injecting the ligand solution, a solution containing the same amount of ethanol (0.2%) was injected as a solvent control to distinguish between the response to the ligand and the response to the ethanol. Both the ethanol and PK11195 solutions were injected over bare SiO_2 and DTSP-ANTA-Cu^{2+} modified gold to check for any interaction with the surface. The interaction of PK11195 with TSPO/DMPC/DMPE (9:1) bilayers was compared with DMPC/DMPE (9:1) bilayers formed on SiO_2 because it was not possible to form them on Au-DTSP-ANTA-Cu^{2+} without the immobilised TSPO.

Frequency and dissipation data were collected at the fundamental frequency (5 MHz) of the quartz crystal and at 6 additional overtones of the fundamental frequency. Overtones 5, 7, 9, 11, and 13 were normalised and used in analysis. Traces of Δf and ΔD represent the normalised 5th overtone. Sauerbrey thickness and mass were calculated using the QTools analysis software (QSense, Sweden), using the Sauerbrey equation [36]:

$$\Delta\ mass = C/n\ \Delta frequency,$$

where $C = -17.7$ Hz ng/cm^2 for a 5 MHz crystal and n is the overtone number. Statistical analysis to compare bilayer compositions was carried out using a one way ANOVA in GraphPad Prism 5, with a Bonferroni post-hoc test. All errors reported are standard deviations.

2.7. Neutron reflectometry

Polished silicon blocks (80 mm × 40 mm × 15 mm (100) orientation) were used as a solid substrate for the deposition of lipid bilayers described in Section 3.4. The blocks were cleaned in a piranha solution of 1:4:5 (by volume) $H_2O_2/H_2SO_4/H_2O$ at 80 °C for 15–30 min, rinsed thoroughly with ultrapure water, dried with compressed air, then treated for 30 min with UV ozonolysis (caution: piranha solution is a strong oxidant and reacts violently with organic substances). This cleaning treatment results in a natural oxide layer of 7–20 Å thickness and 3–5 Å roughness [37]. Blocks were assembled into solid–liquid sample cells consisting of a Teflon sample reservoir and aluminium fronting and backing plates with temperature control through a circulating water bath.

The lipids used for all neutron reflectometry experiments were the chain perdeuterated d_{54}-DMPC and hydrogenated DMPE. Lipid bilayers composed of either d_{54}-DMPC/DMPE (9:1) or d_{54}-DMPC/DMPE (9:1) / PK11195 were formed on the silicon oxide surface by depositing a 0.5 mg/ml solution of SUVs at 45 °C in buffer (10 mM Tris–HCl, 150 mM NaCl pH 7.4), then cooled to 25 °C before measurement. Neutron reflectivity data for these bilayer samples were collected on the Platypus time-of-flight neutron reflectometer at the 20 MW OPAL research reactor, Australian Nuclear Science and Technology Organisation (ANSTO), Sydney, Australia [38,39], using a cold neutron spectrum with wavelengths of 2.8 Å–18.0 Å. Reflectivity was measured at angles of 0.8° and 3.0° in D_2O, and 0.6° and 2.5° in CM4 (a mixture of D_2O and H_2O to have an SLD of 4×10^{-6} Å^{-2}) or CMSi (a mixture of D_2O and H_2O to match the SLD of the silicon substrate, 2.07×10^{-6} Å^{-2}) to cover a momentum transfer (Q) range of 0.01–0.23 Å^{-1}. To test ligand

interactions with d_{54}-DMPC/DMPE (9:1), PK11195 at a concentration of 100 μM was injected over the bilayer, incubated for 90 min, and reflectivity data were collected again in D_2O and CMSi solvents.

Silicon blocks (100 mm diameter × 10 mm height) coated with chromium and gold were used for TSPO/lipid bilayer measurements described in Section 3.7. The blocks were cleaned with 2% Hellmanex, rinsed thoroughly with ultra-pure water, isopropanol, and dried under nitrogen. The gold surface of each block used was then modified in order to bind His-tagged TSPO using the methods described in Section 2.6. Blocks were assembled into circular solid–liquid sample cells consisting of a Teflon reservoir, aluminium backing plates, and inlet and outlet valves connected to an HPLC pump for automatic sample injection and solvent exchange. Sample cells were maintained at 25 °C.

The modified gold surfaces in D_2O were measured before 4 ml of 50 μg/ml TSPO in Tris buffer containing 0.5% SDS (wt/vol) was injected and incubated on the surface for 60 min. Excess protein was rinsed off with Tris + 0.5% SDS before measuring the reflectivity of the TSPO/SDS layer. A lipid bilayer was then reconstituted around the TSPO layer by first injecting a solution of 0.1 mg/ml d_{54}-DMPC/DMPE (9:1) vesicles solubilised in 0.035% SDS (wt/vol) in Tris buffer and leaving the mixture to incubate for 60 min. Reconstitution was completed by injecting a 0.1 mg/ml d_{54}-DMPC/DMPE (9:1) vesicle solution, incubating for 60 min, and rinsing with Tris buffer to remove excess vesicles before measuring the reflectivity of the TSPO/lipid bilayer.

Neutron reflectivity measurements at each stage of the construction of a TSPO/lipid bilayer described above were carried out on the SURF reflectometer located at the ISIS spallation neutron source (Rutherford Appleton Laboratories, Didcot, Oxfordshire, UK). Measurements on SURF used neutrons with wavelengths of 0.5 Å–6.8 Å. Reflectivity was measured at angles of 0.35°, 0.8° and 1.8° to cover a Q of 0.01–0.49 $Å^{-1}$. At each stage of sample development the reflectivity was measured in 3 solvent contrasts: D_2O, H_2O, and contrast matched gold (CMAu, nSLD of 4.5×10^{-6} $Å^{-2}$). The bare modified surface was measured in D_2O only.

Reflectivity data from both Platypus and SURF were reduced at the beamline and later modelled using the MOTOFIT analysis program [40]. MOTOFIT uses the Abeles matrix method to produce a slab model of the reflectivity data with the thickness, SLD, solvent penetration and roughness of each layer. Data from multiple solvent contrasts for each sample were co-refined to arrive at one model to fit all data. The volume fraction of each component was calculated using the theoretical SLDs given in Table S1 of the Supplementary Material. Errors given are the standard deviations reported by MOTOFIT.

3. Results and discussion

3.1. PK11195 in lipid monolayers

We first assessed the possible interaction of PK11195 with lipids in monolayers at the air–water interface using a Langmuir film balance. A comparison of the pressure-area isotherms of pure DMPC, pure PK11195 and DMPC/PK11195(1:1) is given in Fig. 2. The DMPC isotherm indicates that the monolayer is primarily in the liquid-expanded phase, and does not exhibit any clear phase transitions at this temperature. The PK11195 isotherm indicates that it forms a monolayer at the air–water interface upon compression and is in the liquid-condensed phase at molecular areas below 13 $Å^2$. The pure PK11195 monolayer reaches small values of surface pressure when compared to the pure DMPC monolayer, but is comparable to isotherms obtained for other drug ligands [41]. There is evidence of adsorption of PK11195 to the air–water interface; thus, it has potential to be incorporated into a monolayer of lipids.

The pressure-area isotherm of a mixed DMPC/PK11195 (1:1) monolayer indicates that the inclusion of PK11195 in the DMPC monolayer caused a shift of the DMPC isotherm to smaller molecular areas, and a shift from the liquid-expanded to the liquid-condensed phase at molecular areas below 60 $Å^2$ (Fig. 2). The same total amount of DMPC was deposited on the surface in each case, so it is likely that the PK11195 is causing the DMPC monolayer to become more compact, as illustrated in Fig. 2 inset. At surface pressures of 35 mN/m, similar to a lipid bilayer [42], the area/molecule of the DMPC monolayer is 58 $Å^2$, while the area/DMPC molecule of the DMPC/PK11195 (1:1) monolayer is 44 $Å^2$.

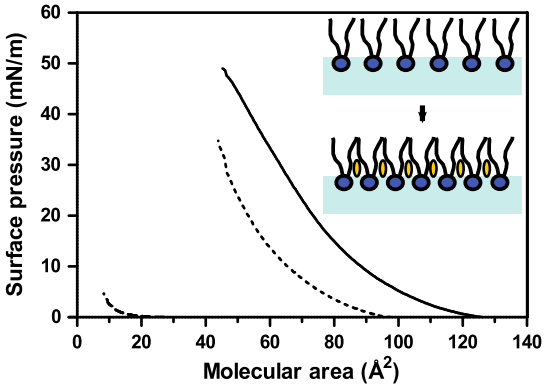

Fig. 2. Pressure-area isotherms of DMPC and PK11195 monolayers. The pressure-area isotherms of pure DMPC (solid line), pure PK11195 (long dashes), and a 1:1 (mol/mol) mixture of DMPC and PK11195 (short dashes) were measured with a Langmuir film balance. Inset is a schematic of a DMPC/PK11195 (1:1) monolayer at the air-water interface. Yellow molecules represent PK11195.

This effect has been observed in mixed DMPC/cholesterol monolayers, as the cholesterol increases the order of the acyl chains and condenses the monolayer [43]. In addition, there is evidence that hexadecanol can replace cholesterol in DMPC monolayers to produce the same or greater effect [44]. In general, a drug that condenses a lipid monolayer is likely to insert among the acyl chains, increasing their order and packing [45]. Given that other drug ligands and organic compounds [46] can exert a similar effect to cholesterol, it is likely that PK11195 is also inserted into the acyl chain region of the DMPC monolayer to cause a decrease in molecular area of the DMPC.

3.2. Incorporation of PK11195 into lipid bilayers

Next, we pre-incorporated the TSPO ligand PK11195 into lipid vesicles to investigate (using QCM-D) whether a planar lipid bilayer formed from mixed lipid/PK11195 vesicles differed from one formed using lipid only vesicles. The change in frequency (Δf) and dissipation (ΔD) measured by QCM-D after stable planar bilayer formation is given in Table 1 for each vesicle composition. Typical traces of Δf and ΔD during bilayer formation are given in Fig. S1 and are in good agreement with QCM-D data for similar lipid compositions [47].

In the case of both DMPC and DMPC/DMPE (9:1) vesicles, the incorporation of PK11195 produced bilayers with a final Δf and ΔD that was smaller than the lipid only bilayers ($p < 0.05$) (Table 1). The smaller ΔD of the bilayers containing PK11195 indicates that the presence of the ligand produces a more rigid bilayer; similar to an effect observed when glycolipids were incorporated into egg PC bilayers [48]. The increased

Table 1
QCM-D measurements of lipid bilayers with and without PK11195. The mean change in frequency and dissipation associated with the formation of bilayers with and without PK11195. The change in mass is calculated from the change in frequency using the Sauerbrey equation.

Composition	Δ Frequency (Hz)	Δ Dissipation (10^{-6})	Δ Mass (ng/cm^2)
DMPC	−24 ± 1.2	0.9 ± 0.2	425 ± 21
DMPC/PK11195 (1:1)	−22 ± 0.9	0.2 ± 0.2	389 ± 16
DMPC/DMPE (9:1)	−26 ± 0.6	0.9 ± 0.2	460 ± 11
DMPC/DMPE/ PK11195 (9:1:10)	−24 ± 0.6	0.5 ± 0.2	425 ± 11

rigidity of the mixed lipid/PK11195 bilayers may represent a decrease in fluidity, an effect that has been observed when cholesterol is incorporated into PC bilayers [49]. It is likely that the fluidity of the lipid/PK11195 bilayers was reduced due to increased ordering of the lipid chains [50], an interpretation that is in agreement with the condensing effect of PK11195 on DMPC monolayers we observed in Fig. 2.

The final Δf for bilayers containing PK11195 was smaller than for lipid only bilayers, giving a smaller value for Sauerbrey mass (Table 1). The deposited mass measured by QCM-D includes coupled water due to hydration of the bilayer, and it is difficult to distinguish the mass due to lipid from the mass due to hydration without the use of optical techniques [51]. Thus, it is possible that the decrease in Sauerbrey mass of the lipid/PK11195 bilayers could be due to a smaller mass of the bilayer itself or to decreased hydration of the bilayer compared to lipid only.

If the measured mass purely reflected the mass of the bilayer, then a greater mass for the lipid/PK11195 bilayer would be expected if it were condensed compared to a lipid only bilayer, as the surface could accommodate more molecules [48]. Therefore, it is possible that the smaller mass of the lipid/PK11195 bilayers is due to a decrease in hydration, just as the addition of cholesterol to lipid bilayers results in decreased interchain hydration of the lipid [49,50,52]. A decrease in hydration of the lipid chain region would be consistent with increased ordering of the lipid [50], as indicated by the increased rigidity of bilayers containing PK11195.

The differences between the bilayers with and without PK11195 indicate that the PK11195 has been incorporated into the bilayer, causing a change in the bilayer structure. The difference in structure between a lipid bilayer with and without PK11195 was further investigated using neutron reflectometry and is discussed in Section 3.4.

3.3. Interaction of PK11195 with lipid bilayers

The above results indicate that PK11195 interacts with lipid molecules and can be pre-incorporated into lipid monolayers and bilayers. Hence, we aimed to further investigate this interaction by looking at whether PK11195 in solution would interact with an already formed supported lipid bilayer. The interaction of PK11195 with bilayers composed of DMPC/DMPE (3:2) and DMPC/DMPE/cholesterol (8:1:1), chosen to reflect the major components of the outer mitochondrial and plasma membranes respectively, were tested in addition to the DMPC/DMPE (9:1) and DMPC/DMPE/PK11195 (9:1:10) bilayers used in Section 3.2.

The peak Δf, ΔD, and Sauerbrey mass during exposure of each bilayer composition to PK11195 is given in Table 2. There was a significantly greater Δf and ΔD when PK11195 was injected over all lipid bilayer compositions when compared to the bare surface ($p < 0.05$), indicating that the interaction was particular to the lipids rather than SiO_2.

The magnitude of the interaction differed between some lipid compositions (Table 2). In particular, there was a significantly smaller PK11195 induced Δf for bilayers already containing PK11195 when compared to those without ($p < 0.05$). This may indicate that the bilayer is already occupied by pre-incorporated PK11195 leaving little room for further incorporation of PK11195 from solution. The additional mass after exposure of DMPC/DMPE/PK11195 (9:1:10) bilayers to PK11195 was approximately half that of the other lipid compositions (Table 2). Hence, it appears that PK11195 is present in the bilayer after pre-incorporation and lowers the amount of PK11195 that interacts with the bilayer from solution.

The PK11195 induced Δf did not differ between the DMPC bilayers with varying amounts of DMPE (Table 2). There was a significantly larger response for DMPC/DMPE/cholesterol (8:1:1) than for DMPC/DMPE (3:2) ($p < 0.05$), but no statistically significant difference between the PK11195 induced Δf in DMPC/DMPE/cholesterol (8:1:1) vs. DMPC/DMPE (9:1) bilayers. However, the Δf between DMPC/DMPE (9:1) and DMPC/DMPE (3:2) are similar, and considering there is a difference between DMPC/DMPE (3:2) and DMPC/DMPE/cholesterol (8:1:1) it is possible that with further investigation a difference between DMPC/DMPE (9:1) and DMPC/DMPE/cholesterol (8:1:1) may emerge.

Table 2
QCM-D measurements of the interaction of PK11195 with lipid bilayers. The mean peak change in frequency, dissipation and Sauerbrey mass of lipid bilayers and bare SiO_2 associated with exposure to PK11195.

Composition	Δ Frequency (Hz)	Δ Dissipation (10^{-6})	Δ Mass (ng/cm^2)
SiO_2 surface	−0.2 ± 0.3	0.01 ± 0.02	4 ± 5
DMPC/DMPE (9:1)	−1.5 ± 0.1	0.90 ± 0.13	27 ± 2
DMPC/DMPE/PK11195 (9:1:10)	−0.8 ± 0.3	0.87 ± 0.13	14 ± 5
DMPC/DMPE/chol (8:1:1)	−1.9 ± 0.1	0.91 ± 0.03	34 ± 2
DMPC/DMPE (3:2)	−1.4 ± 0.2	1.08 ± 0.17	25 ± 4

The Δf and ΔD after exposure of lipid bilayers to PK11195 tended to peak very soon after injection of the ligand (Fig. 3, point B). This indicates that there is rapid association of the PK11195 to the lipid bilayer [53], and is unlikely to purely reflect a change in the viscosity of the bulk solvent as the effect was not present on the bare surface. After reaching a peak, both the Δf and ΔD signals began to move towards pre-PK11195 values (Fig. 3, point B to C). This effect was not observed when the bilayers were exposed to 0.2% ethanol or buffer only for the same amount of time, indicating that it is not due to drift in the signal.

The changes in Δf and ΔD values during incubation (Fig. 3, point B to C) indicate a process of PK11195 association and incorporation into the bilayer [54,55]. The initial peak signals indicate the association of PK11195 with the surface of the bilayer, as a layer of PK11195 on top of the bilayer is expected to cause increased mass and an increased ΔD [55]. The decrease in ΔD values over time (Fig. 3, point B to C) indicates a structural rearrangement of the bilayer and associated PK11195 [56], and may reflect PK11195 being gradually incorporated from the surface of the bilayer into the bilayer [54,55]. The gradual increase in Δf values (Fig. 3, point B to C) indicates a slight loss of mass from the surface, possibly because of a loss of water from the bilayer as PK11195 is incorporated, or the dissociation of excess PK11195 from the bilayer surface as the binding and incorporation reach equilibrium [57].

After PK11195 and ethanol had been completely rinsed from the lipid bilayers, Δf and ΔD values tended to be higher and lower, respectively, than before exposure to PK11195 (Fig. 3, point D). The slight increase in Δf values indicates a small loss of mass, and is similar to the

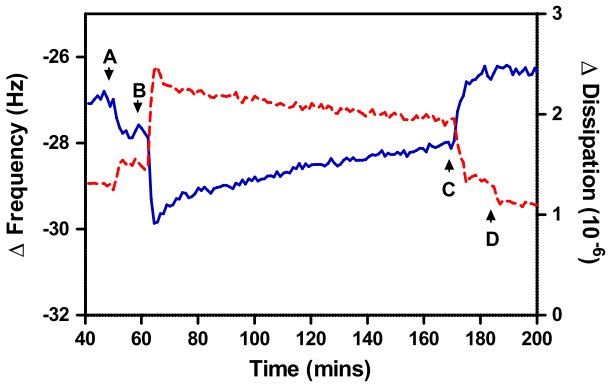

Fig. 3. QCM-D trace of PK11195 interaction with a lipid bilayer. A typical trace of frequency (f) (blue solid line) and dissipation (D) (red dashed line) during the exposure of a lipid bilayer to 0.2% ethanol and 100 μM PK11195. The trace starts after the formation of a stable DMPC/DMPE (9:1) bilayer on SiO_2. There are a small decrease in f and increase in D when 0.2% ethanol is introduced (point A). Subsequent injection of PK11195 (point B) results in a further decrease in f and increase in D, both of which peak soon after exposure to PK11195, followed by a gradual return towards 0.2% ethanol values during incubation. When the PK11195 (point C) and ethanol (point D) are rinsed away with buffer, the f and D signals appear to be slightly higher and lower, respectively, than before exposure to PK11195.

observed effect of pre-incorporating PK11195 into bilayers. The same was the case for ΔD values, with a smaller final ΔD indicating a more rigid bilayer, as for bilayers with pre-incorporated PK11195. Overall, the changes in Δf and ΔD values during exposure of lipid bilayers to PK11195 indicate that it associated with the bilayer and caused some structural change [54,55,57].

While the PK11195 induced ΔD was greater for lipid bilayers than for the bare surface (Table 2), the change did not differ between lipid compositions of the non-PK11195 pre-incorporated bilayers. This indicates that the PK11195 adsorbs to lipid bilayers in a similar way regardless of lipid composition [54]. The ΔD is likely to reflect a change in overall structure of the adsorbed layer, and possibly the addition of a PK11195 layer on the surface of the lipid bilayer. The consistent ΔD across lipid bilayer compositions (Table 2) indicates that the mode of interaction is the same, while the difference in Δf indicates that the amount of associated ligand differs between lipid compositions [54,55]. The effect of PK11195 interaction on lipid bilayer structure was investigated further with neutron reflectometry, and results are presented in Section 3.4.

3.4. Structure of lipid bilayers with PK11195

The thickness and composition of a d_{54}-DMPC/DMPE (9:1) bilayer before and after exposure to PK11195, and a d_{54}-DMPC/DMPE (9:1) bilayer with pre-incorporated PK11195, were investigated with neutron reflectometry to further characterise the changes seen with QCM-D. The reflectivity profiles of each system in D_2O are given in Fig. 4. The reflectivity profiles and fits at each solvent contrast measured are given in Fig. S2 (d_{54}-DMPC/DMPE (9:1)), Fig. S3 (d_{54}-DMPC/DMPE (9:1) / PK11195) and Fig. S4 (d_{54}-DMPC/DMPE (9:1) + PK11195) of the Supplementary Material. In each case the bilayer itself was fitted using all solvent contrasts to a three layer model consisting of the inner lipid headgroup, lipid chain region, and the outer lipid headgroup. The details of modelled parameters for each sample are given in Table 3, and Table S2 of the Supplementary Material.

The volume fractions of lipid, solvent and PK11195 in each layer were calculated from the fitted nSLDs and the molecular nSLDs using the equation:

$$\rho_{layer} = \phi_{lipid}\rho_{lipid} + \phi_{PK11195}\rho_{PK11195} + \phi_{solvent}\rho_{solvent}.$$

The volume fraction of PK11195 in the lipid headgroups, if it was present in this region, could not be calculated due to the similarity of the nSLD of PK11195 to the headgroups (Supplementary Table S1). It was also difficult to distinguish the contribution of PK11195 to the nSLD of the headgroup regions from the solvent penetration.

The nSLD of the lipid chain region of the d_{54}-DMPC/DMPE (9:1) / PK11195 bilayer, and the d_{54}-DMPC/DMPE (9:1) bilayer after exposure to PK11195, was reduced compared to that of the d_{54}-DMPC/DMPE (9:1) bilayer (Fig. 4B). In each case the nSLD of the chain regions indicated a volume fraction of approximately 10% PK11195 (Table 3). A similar volume fraction of PK11195 in the case of both pre-incorporation and interaction with a pre-formed bilayer indicates that there may be a preferred molar ratio for the lipid to PK11195 interaction.

The surface excess (Γ) of both PK11195 and lipid was calculated using the equation:

$$\Gamma = (\phi \times d \times M)/(V \times N_A)$$

where φ is volume fraction, d is thickness, M is molar mass, and V is molecular volume. Molecular volumes of 1101 Å^3 [58] for lipid and 323 Å^3 for PK11195 (calculated with the Molinspiration Property Calculator [59]) were used. The surface excesses of PK11195 and lipid (Table 3) for the d_{54}-DMPC/DMPE (9:1) bilayer after interaction with PK11195 are close to the Sauerbrey mass values calculated from QCM-D results (Tables 1 and 2). The calculated surface excess gives a PK11195 to lipid molar ratio of 1:9.6, which is similar to the ratio of 1:8.2 from QCM-D results. Likewise, the surface excesses of PK11195 and lipid for the d_{54}-DMPC/DMPE (9:1)/PK11195 bilayer give a PK11195 to lipid molar ratio of 1:10.3. Results from both neutron reflectivity and QCM-D are in good agreement and further indicate a preferred PK11195 to lipid molar ratio for association. The consistent molar ratio of PK11195 incorporation may also explain why there was less binding of PK11195 from solution with bilayers already containing PK11195 observed in QCM-D experiments.

The solvent volume fraction in the chain region of the d_{54}-DMPC/DMPE (9:1)/PK11195 bilayer was slightly higher than that of the d_{54}-DMPC/DMPE (9:1) bilayer (Table 3), which could indicate

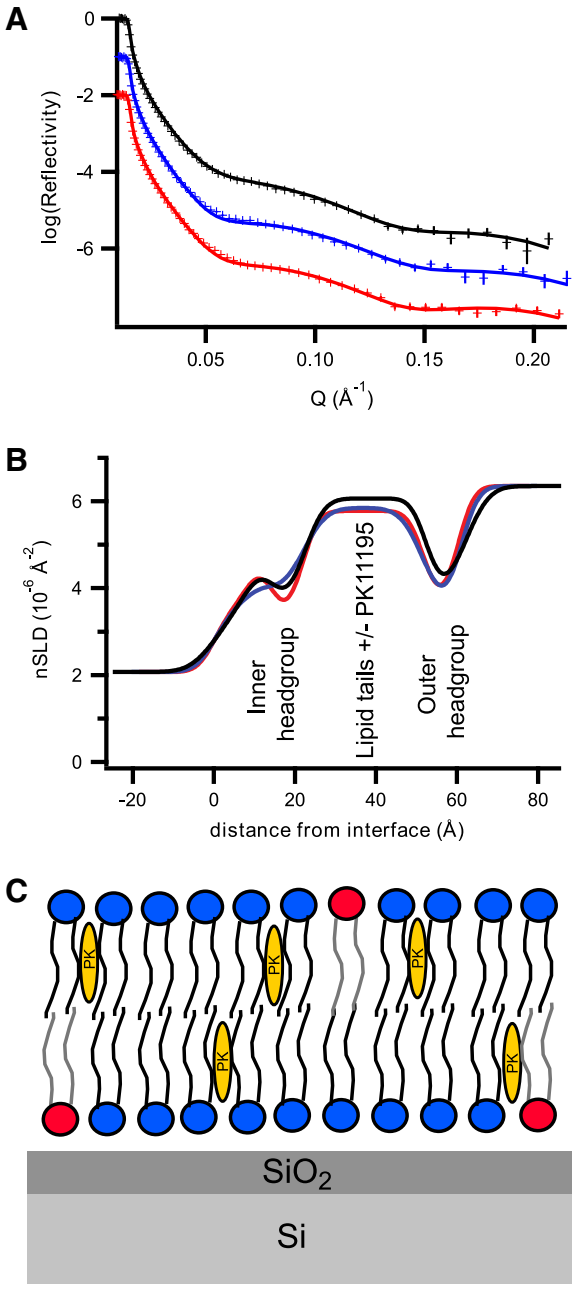

Fig. 4. Neutron reflectivity measurements of lipid bilayers with PK11195. (A) Neutron reflectivity profiles of a d_{54}-DMPC/DMPE (9:1) bilayer before (black) and after (red) exposure to 100 μM PK11195, and a d_{54}-DMPC/DMPE (9:1) /PK11195 bilayer (blue) measured in D_2O. Points and error bars are measured data, and lines are fits to the data. (B) Comparison of scattering length density profiles of lipid bilayers with and without PK11195 in D_2O. (C) Schematic of the structure of a d_{54}-DMPC/DMPE (9:1) bilayer with incorporated PK11195.

Table 3
Neutron reflectivity measurements of lipid bilayers with and without PK11195. Modelled parameters derived from neutron reflectivity data for a d_{54}-DMPC/DMPE (9:1) bilayer before and after exposure to PK11195, and a d_{54}-DMPC/DMPE (9:1) /PK11195 bilayer. The thickness (d), volume fraction (φ) and surface excess (Γ) are given for each layer.

	d (Å)	φ_{lipid}	$\varphi_{solvent}$	$\varphi_{PK11195}$	Γ_{lipid} ng/cm^2	$\Gamma_{PK11195}$ ng/cm^2
d_{54}-DMPC/DMPE (9:1)						
Inner headgroup	9 ± 2	0.74	0.26	–	520 ± 61	–
Chain region	30 ± 3	0.98	0.02	–		
Outer headgroup	9 ± 2	0.66	0.34	–		
d_{54}-DMPC/DMPE (9:1) + 100 μM PK11195						
Inner headgroup	8 ± 2	0.76	0.24	–	457 ± 53	
Chain region	30 ± 3	0.88	0.02	0.10		23 ± 3
Outer headgroup	9 ± 2	0.66	0.34	–		
d_{54}-DMPC/DMPE (9:1) /PK11195						
Inner headgroup	9 ± 2	0.64	0.36	–	471 ± 55	
Chain region	31 ± 3	0.87	0.05	0.08		22 ± 3
Outer headgroup	9 ± 2	0.75	0.25	–		

higher hydration of the chain region or less complete bilayer surface coverage [60]. The solvent penetration into the headgroups of the d_{54}-DMPC/DMPE (9:1) /PK11195 bilayer indicates a similar level of hydration as the d_{54}-DMPC/DMPE (9:1) bilayer (Table 3). The nSLD and solvent penetration in the lipid headgroups of d_{54}-DMPC/DMPE (9:1) after exposure to PK11195 remained essentially the same as before exposure (Table 3).

The thickness of each layer of the d_{54}-DMPC/DMPE (9:1) /PK11195 bilayer is essentially the same (within error) as that of the d_{54}-DMPC/DMPE (9:1) bilayer (Table 3). The inner and outer head groups of both compositions had a thickness of 9 ± 2 Å, while the chain regions of d_{54}-DMPC/DMPE (9:1) and d_{54}-DMPC/DMPE (9:1) /PK11195 were 30 ± 3 Å and 31 ± 3 Å thick respectively. The comparison of QCM-D data for lipid bilayers presented in Section 3.2 indicates that the incorporation of PK11195 caused bilayers to become more rigid at 37 °C, and possibly shifts fluid bilayers towards the gel phase. A shift towards the gel phase is typically accompanied by an increase in acyl chain thickness [58]. However, an increase in thickness was not observed in the neutron reflectivity data. This may be because the data were measured at 25 °C rather than 37 °C, which was necessary for better bilayer stability on the silicon surface over the required measurement times. At 25 °C the DMPC/DMPE lipid mixture is likely to be in a mixed gel and liquid crystalline phase [61], with an acyl chain thickness that is approaching the theoretical maximum [62,63]. Hence, the incorporation of PK11195 may have a less pronounced effect than at 37 °C. It is also possible that any change in thickness may be too small to detect given the error in the measurement.

The thickness of the d_{54}-DMPC/DMPE (9:1) bilayer was also unchanged by interaction with PK11195, as was the case for pre-incorporated PK11195 bilayer (Table 3). The QCM-D data for PK11195 interaction with lipid bilayers (Section 3.3) indicated that a layer of PK11195 may have been adsorbed to the surface of the bilayer initially, before incorporating into the bilayer. However, an additional layer above the lipid bilayer to represent PK11195 could not be fitted to the neutron reflectivity data. It is possible that if there was a layer of PK11195 on the bilayer surface it did not have enough SLD contrast to be detected. It is also possible that the PK11195 initially adsorbed to the surface of the bilayer had either been incorporated into the bilayer or disassociated by the time of measurement, as measurements were made after a 90 min incubation period.

Overall, we detected a change in composition between the d_{54}-DMPC/DMPE (9:1) and d_{54}-DMPC/DMPE (9:1) /PK11195 bilayers using neutron reflectometry, but observed no significant change in bilayer thickness. Additionally, it appears that PK11195 is incorporated into a d_{54}-DMPC/DMPE (9:1) bilayer from solution in much the same way as when pre-incorporated into lipid vesicles before planar bilayer formation. A consistent PK11195 volume fraction of around 10% in the lipid chain regions of both systems indicates that there is a preferred ratio of lipid to PK11195. The combination of our results from Langmuir monolayers, QCM-D and NR provide evidence that PK11195 is incorporated into lipid bilayers and monolayers and suggest an interaction with lipids that is similar to that of cholesterol. The decreased area/molecule and increased rigidity of monolayer and bilayers with PK11195 suggest that the ligand is incorporated into the lipid chains, increasing their order and reducing fluidity, as observed previously for cholesterol [64]. It is interesting to note that Miccoli et al. [18] found an increase in mitochondrial membrane fluidity after exposure to 10 nM PK11195 for 24 h, which was regulated via binding to TSPO. Our results may differ because they reflect a direct and acute interaction between the ligand and lipid in the absence of TSPO, and at a higher ligand concentration. Other recent studies have highlighted the effect of small molecule incorporation on lipid membrane properties and the implications this has in disease [64], and our results suggest this as one mechanism through which PK11195 exerts its TSPO-independent effects at micromolar concentrations.

3.5. Reconstitution of mouse TSPO into a supported lipid bilayer

Protein/lipid bilayers were formed using the general method illustrated in Fig. 5. The first step in reconstituting TSPO into a DMPC/DMPE (9:1) bilayer is immobilising the protein to a modified gold surface, which we followed by measurement with QCM-D. Our results indicate that the TSPO was immobilised to the Au-DTSP-ANTA-Cu^{2+} surface via its His-tag in a reversible manner, and that TSPO binding was displaced by imidazole (Fig. S5 in Supplementary Material).

We then monitored the complete process of forming a TSPO and DMPC/DMPE (9:1) bilayer (Fig. 6). The Δf, ΔD, Sauerbrey mass and Sauerbrey thickness values at the major stages of this process are given in Table 4. The small decrease in Δf and increase in ΔD observed after the introduction of 0.5% SDS (Fig. 6, point A) indicates some adsorption of SDS to the crystal surface, an effect which has also been observed for *n*-Dodecyl β-D-maltoside (DDM) on a gold surface with the same modifications [23].

The decrease in Δf as a result of incubating TSPO on the surface indicates adsorption of the protein (Fig. 6, point B to D). The molecular area of a TSPO monomer is estimated to be 540 Å^2, based on a molecular area of 1080 Å^2 for a dimer of its homologue TspO from *Rhodobacter sphaeroides* [65]. The molecular weight of the engineered TSPO is 21 kDa. Using these values for molecular weight and area of the TSPO, a full coverage monolayer of TSPO would theoretically result in a Δf of −37 Hz. The Δf due to TSPO/SDS adsorption was −34 Hz (Fig. 6, point B to D), which is close to the expected value. This Δf value is comparable to other studies of protein adsorption using QCM-D, which were in the range of −13 to −54 Hz depending on the molecular weight and molecular area of the protein [27–29].

The ΔD value reaches 1.9×10^{-6} after protein adsorption (Table 4). Other studies have reported ΔD values as high as 15.8×10^{-6} for a viscoelastic protein layer, and 1.5×10^{-6} for a more rigid protein layer

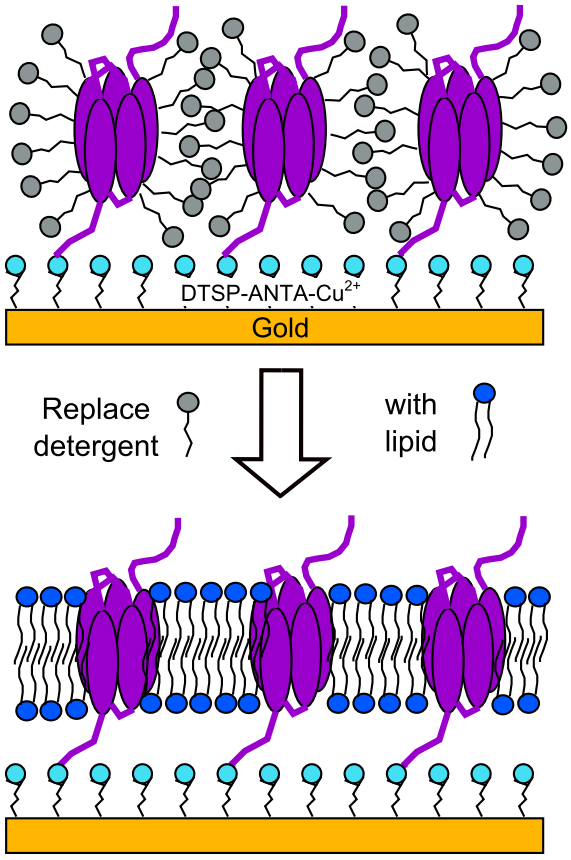

Fig. 5. Schematic of the process of protein/lipid bilayer formation with TSPO. The gold surface is modified to allow the reversible binding of His-tagged proteins by first exposing to dithiobis (*N*-succinimidyl propionate) (DTSP) to create a *N*-hydroxy succinimide (NHS) ester functionalised surface. Next, the NHS surface is coupled with nitrilotriacetic acid groups bearing a terminal amino group (ANTA). The surface is activated by complexation of Cu^{2+}, and is ready to bind His-tagged protein. TSPO solubilised in detergent is then immobilised to the modified gold surface via its His-tag. The detergent is gradually replaced by lipid, and a lipid bilayer is reconstituted around the immobilised TSPO.

[66]. Applying the Sauerbrey equation to calculate the thickness of the TSPO/SDS layer gives a value of 5.7 nm, which is in the range expected for a protein such as TSPO that spans a phospholipid bilayer membrane [10].

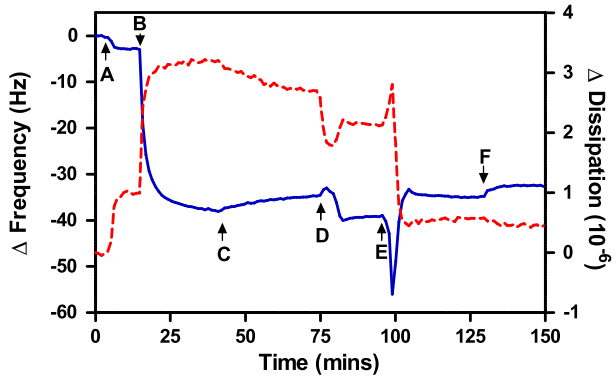

Fig. 6. QCM-D trace of the process of TSPO/DMPC/DMPE (9:1) bilayer formation. A typical trace of frequency (*f*) (blue solid line) and dissipation (*D*) (red dashed line) during the formation of a TSPO/DMPC/DMPE (9:1) bilayer. The process commenced with injection of buffer containing 0.5% SDS (A), followed by injection of TSPO in 0.5% SDS (B) which was allowed to incubate on the surface before rinsing off excess protein (C). The reconstitution of lipid around the protein started by injecting a solution of DMPC/DMPE (9:1) vesicles solubilised in SDS (D). To complete the reconstitution process a solution of DMPC/DMPE (9:1) vesicles was injected (E), followed by rinsing to remove excess vesicles (F).

We reconstituted a DMPC/DMPE (9:1) bilayer around immobilised TSPO by gradually replacing SDS with lipid. When SDS solubilised lipid vesicles were injected there was a decrease in Δf and ΔD (Fig. 6, point D). This may indicate that space between bound TSPO/SDS was being filled by lipid molecules, and that the TSPO/SDS/lipid layer was beginning to adopt a more rigid structure. A solution of DMPC/DMPE (9:1) vesicles was then injected to complete the removal of SDS (Fig. 6, point E). The spike in Δf and ΔD observed at this point indicates the adsorption and then rupture of lipid vesicles, as seen when forming lipid only bilayers on a SiO_2 surface [33].

The stable Δf value of TSPO/DMPC/DMPE (9:1) was slightly higher than TSPO/SDS, with a lower ΔD value (Table 4), suggesting that the TSPO/DMPC/DMPE (9:1) layer had a smaller mass than the TSPO/SDS layer, and was more rigid. It is likely that replacing SDS micelles with a lipid bilayer caused the layer to become more rigid and TSPO to adopt a different conformation, as reconstituting TSPO into a more natural lipid layer is likely to result in refolding of the protein [30].

We also expect a TSPO/DMPC/DMPE (9:1) layer to have a smaller mass than a TSPO/SDS layer at constant protein coverage, if the volume of the layer not occupied by protein was entirely composed of SDS or lipid molecules. The protein surface coverage was approximately 50%, based on a mass of 537 ng/cm^2, and molecular areas of 540 Å^2 for TSPO and 50 Å^2 on average for DMPC/DMPE (9:1). The Sauerbrey thickness of the TSPO/DMPC/DMPE (9:1) layer is 5.1 nm, which is reasonable given the thickness of a DMPC/DMPE (9:1) bilayer (Section 3.4), the estimated thickness of TSPO in the membrane plane [65], and values reported for other protein/lipid bilayers on the same surface [23]. Overall, our results indicate that TSPO in SDS was successfully immobilised to an Au-DTSP-ANTA-Cu^{2+} surface, and that gradual replacement of SDS with DMPC/DMPE (9:1) resulted in the formation of a TSPO/DMPC/DMPE (9:1) layer of expected mass and thickness.

3.6. Ligand interactions of reconstituted TSPO

We first assessed the activity of recombinant TSPO by its ability to bind ^{3}H-PK11195 when reconstituted into DMPC/DMPE (9:1) liposomes (Fig. 7). The Kd value of 7.3 nM was similar to that obtained for TSPO proteoliposomes elsewhere [30], and is in the affinity range typically reported for PK11195 binding to TSPO in native membrane preparations [1].

We then examined the interaction of PK11195 with reconstituted TSPO/DMPC/DMPE (9:1) bilayers, formed as described in Section 3.5, using QCM-D. Changes in *f* and *D* during exposure to PK11195 are given in Table 5. There was no significant difference in either the Δf or ΔD responses to ethanol between the surface conditions. However, exposure of TSPO/DMPC/DMPE (9:1) bilayers to PK11195 caused a significantly larger Δf when compared to the bare Au-DTSP-ANTA-Cu^{2+} surface or DMPC/DMPE (9:1) bilayers ($p < 0.0001$). This indicates that the presence of TSPO changed the interaction between the Au-DTSP-ANTA-Cu^{2+} surface or DMPC/DMPE (9:1) bilayer and PK11195.

The response is much larger than expected for PK11195 binding to the TSPO. The change in mass if there were one to one binding between PK11195 and TSPO, even at a protein surface coverage of 100%, would result in a Δf of less than −1 Hz. The unexpectedly large Δf could be due to ligand-induced conformational changes of the TSPO, as similar observations were made in QCM-D studies of ligand binding to oestrogen receptors [28,29] and glucose/galactose receptors [27] immobilised to gold. In these studies, the magnitude of Δf varied with different ligands, and they hypothesised that the larger than expected Δf responses were due to ligand-induced conformational changes of the protein [27–29]. It has been suggested that TSPO acts as a cholesterol transport channel, and that binding of ligands such as PK11195 may drive the conformational changes necessary for TSPO to transport cholesterol [67]. There is also evidence that PK11195 stabilises the tertiary fold of isolated TSPO in detergent micelles [8]. Hence, the response we

Table 4
QCM-D measurements during the formation of a TSPO/lipid bilayer. The frequency and dissipation response of a Au-DTSP-ANTA-Cu^{2+} coated quartz crystal was measured after exposure to 0.5% SDS, after the immobilisation of TSPO/SDS, and after the formation of a TSPO/DMPC/DMPE (9:1) bilayer. The mass and thickness were calculated using the Sauerbrey equation. Values given are means ± SD of at least 7 independent measurements.

Composition	Δ Frequency (Hz)	Δ Dissipation (10^{-6})	Δ Mass (ng/cm^2)	Δ Thickness (nm)
SDS only	−2 ± 1	1.0 ± 0.2	41 ± 9	0.4 ± 0.1
TSPO/SDS	−34 ± 2	1.9 ± 0.3	593 ± 41	5.7 ± 0.4
TSPO/lipid	−30 ± 2	0.5 ± 0.2	537 ± 38	5.1 ± 0.4

observed may reflect the conformational changes of TSPO suggested by others upon exposure to PK11195.

The large Δ*f* could also be the result of increased water content of the TSPO/DMPC/DMPE (9:1) bilayer, possibly via a change in lipid bilayer hydration or in conformation of TSPO. For example, the opening of TSPO channels in the TSPO/DMPC/DMPE (9:1) bilayer could increase the amount of water penetrating into the protein/lipid bilayer, thereby increasing its mass.

The Δ*D* as a result of PK11195 exposure was significantly greater for the TSPO/DMPC/DMPE (9:1) bilayer as compared to the Au-DTSP-ANTA-Cu^{2+} surface ($p < 0.01$), but no different from the DMPC/DMPE (9:1) bilayer (Table 5). This suggests that the effect of PK11195 on Δ*D* is not specific to a bilayer containing TSPO, and may reflect an effect on the lipid. Data presented in Section 3.3 suggest an interaction between PK11195 and lipid bilayers, albeit with a significantly smaller Δ*f* than in the presence of TSPO. It is likely that the interaction between PK11195 and lipid makes a small contribution to the overall Δ*f* response of the TSPO/DMPC/DMPE (9:1) to PK11195 exposure, and that the contribution of lipid-PK11195 interaction to Δ*D* is indistinguishable from that of TSPO-PK11195 interaction. Previous studies of small molecule binding to immobilised protein have not measured Δ*D* [27–29]; therefore, it is difficult to make a comparison.

3.7. Characterisation of surface immobilised TSPO with neutron reflectometry

We have characterised the structure of immobilised TSPO on an Au-DTSP-ANTA-Cu^{2+} surface using neutron reflectometry. The reflectivity of surface immobilised TSPO in SDS is given in Fig. 8, with the corresponding SLD profiles. The data were fitted to a five layer model, including the SiO_2, Cr, Au and DTSP-ANTA-Cu^{2+} layers, and one layer for the TSPO (Table S3 in Supplementary Material).

The thickness of the DTSP-ANTA-Cu^{2+} modification was 14 ± 2 Å, which is close to the estimated value of 10 Å [23,26], and the range expected from the dimensions of the molecules. The nSLD of the DTSP-ANTA-Cu^{2+} modification was 2.67×10^{-6} Å^{-2}, which is within the range of theoretical nSLDs of each component (DTSP = 3.40×10^{-6} Å^{-2}, ANTA = 2.21×10^{-6} Å^{-2}, and $CuSO_4$ = 4.86×10^{-6} Å^{-2}). The thickness and SLD of the modification layer did not change significantly with the addition of TSPO, and co-refinement of data taken at multiple solvent contrasts revealed a solvent penetration of approximately 5%.

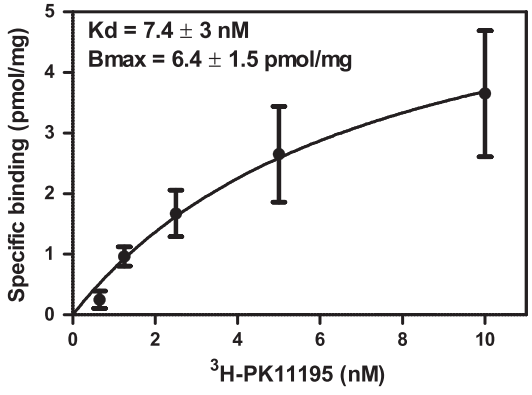

Fig. 7. Saturation isotherm of ^{3}H-PK11195 binding to TSPO proteoliposomes. TSPO was reconstituted into DMPC/DMPE (9:1) liposomes in a 4:1 (w/w) lipid to protein ratio. There is specific binding to proteoliposomes, whereas no specific binding was detected for liposomes without TSPO. Scatchard analysis gives a Kd of 7.4 ± 3 nM and Bmax of 6.4 ± 1.5 pmol/mg for proteoliposomes, mean and SD from three independent experiments.

The thickness of immobilised TSPO in SDS modelled from reflectometry data was 51 ± 2 Å (Fig. 8). The thickness of the TSPO/SDS layer estimated from QCM-D data was approximately 57 Å (Section 3.5); however, this estimate from the QCM-D frequency signal also includes coupled SDS and solvent. The low resolution structure of the TspO, the TSPO homologue from *R. sphaeroides*, indicates that the length of a TspO monomer in the membrane is approximately 40 Å [65]. This length represents the transmembrane helix segments of the protein, and does not take into account extramembrane regions [65]. Considering that the TSPO is predicated to span the thickness of the membrane and have short extramembrane loops [10], a thickness of 51 Å for the immobilised TSPO layer is reasonable (Fig. 8).

The surface coverage estimated from reflectivity data was 23%; lower than the 50% coverage estimated by QCM-D (Section 3.5). However, the coverage of protein only is difficult to extract from QCM-D data because of the contribution of SDS, lipid and coupled solvent to the signal. The protein coverage here is slightly lower, but comparable to that reported for the membrane protein OmpF immobilised to gold via thiol bonds [24]. The volume fraction of the TSPO layer was calculated using the SLD for the protein only, and did not explicitly take into account any contribution from the SDS. However, we observed that the SLD of the bulk solvent was slightly altered when SDS was present, so the presence of SDS was taken into account as a contribution to the solvent surrounding the TSPO.

Finally, we attempted to reconstitute a lipid bilayer around the immobilised TSPO layer in order to further characterise ligand interactions of the TSPO in a lipid bilayer. Unlike QCM-D, the success of TSPO/lipid bilayer reconstitution was limited using neutron reflectometry. Results indicate that after incubating with lipid and washing there was very little TSPO remaining on the substrate surface. We hypothesise that the immobilised TSPO layer may not have been stable enough to maintain surface coverage over the large surface area (50 cm^2 compared to the 1 cm^2 surface of a QCM-D crystal) and repeated rinsing necessary for neutron reflectometry experiments. A repeat experiment confirmed the successful formation of the DTSP-ANTA-Cu^{2+} modification and TSPO/SDS layer, but not lipid reconstitution, as before.

This particular His-tag protein immobilisation method has not previously been used for neutron reflectivity measurements, and our results

Table 5
QCM-D measurements of the interaction of PK11195 with TSPO/lipid bilayers. Changes in frequency, dissipation and Sauerbrey mass after exposure of the bare Au-DTSP-ANTA-Cu^{2+} surface, DMPC/DMPE (9:1) bilayer formed on SiO_2, and TSPO/DMPC/DMPE (9:1) to PK11195. Values given are means ± SD of at least 3 independent measurements.

Composition	Δ Frequency (Hz)	Δ Dissipation (10^{-6})	Δ Mass (ng/cm^2)
Bare Au-DTSP-ANTA-Cu^{2+}	0.2 ± 0.2	0.1 ± 0.1	–
DMPC/DMPE (9:1)	−1.5 ± 0.1	0.9 ± 0.1	26 ± 2
TSPO/DMPC/DMPE (9:1)	−8.6 ± 1.7	0.9 ± 0.4	146 ± 29

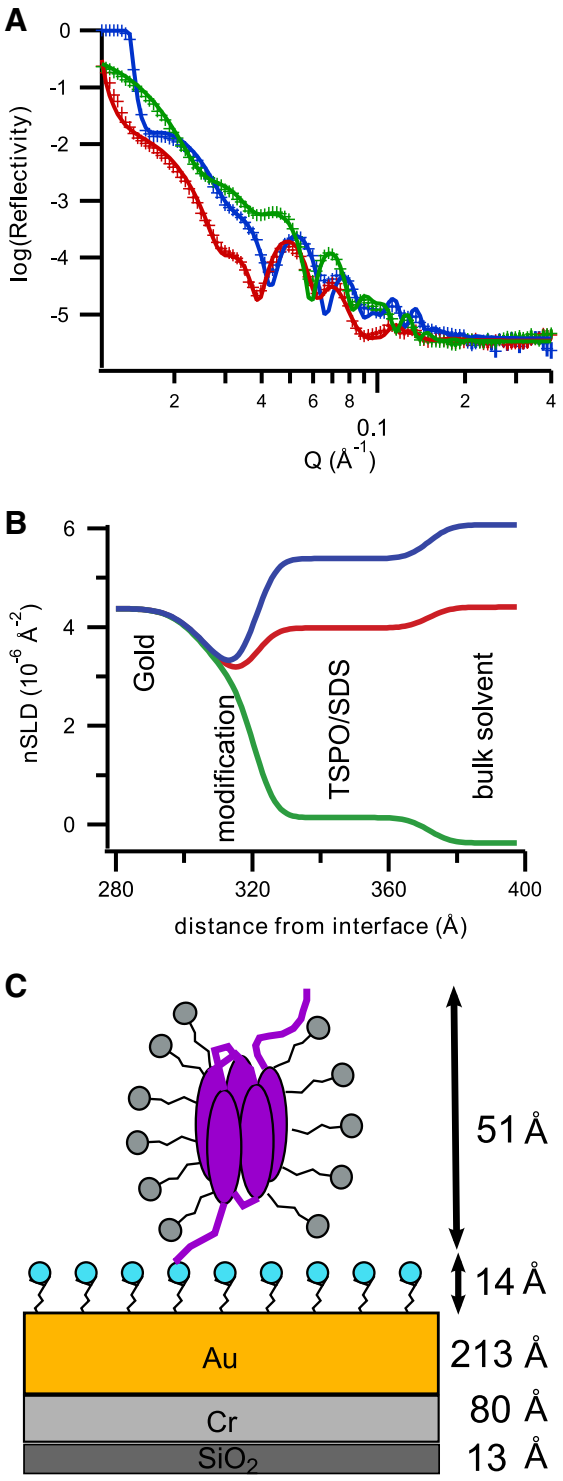

Fig. 8. Neutron reflectivity measurements of a TSPO/SDS layer. (A) Neutron reflectivity profiles of TSPO/SDS immobilised to a DTSP-ANTA-Cu^{2+} modified gold surface measured in D_2O (blue), CMAu (red), and H_2O (green). Points and error bars are the measured data, and lines are the fits to the data. (B) Corresponding scattering length density profile of the TSPO/SDS layer. (C) Schematic of detergent solubilised TSPO immobilised to a gold surface modified with DTSP-ANTA-Cu^{2+} derived from reflectivity data (layers not to scale).

indicate that TSPO was successfully immobilised at a surface coverage that is comparable with other immobilisation techniques used for neutron reflectometry [24]. It was possible to measure the thickness and surface coverage of the immobilised TSPO layer in detergent (Fig. 8), but the use of this method for complete TSPO/lipid bilayer formation for neutron reflectometry experiments revealed problems with up-scaling and prolonged stability. Overall, however, the TSPO/lipid system as it is seems promising for studying the interaction of TSPO with a range of ligands with QCM-D, and with improvement of the system for neutron reflectometry the effect of these interactions on protein conformation could be studied in the future.

4. Conclusions

This work demonstrates the use of QCM-D and neutron reflectometry as part of the systematic characterisation of a ligand's interaction with both its membrane protein target and the surrounding membrane environment. We found evidence that the TSPO ligand PK11195 interacts with lipids, incorporating into lipid bilayer chain regions and causing a change in rigidity. This is the first direct evidence that PK11195 is incorporated into lipid bilayers, while it has been previously assumed that it partitions into membranes to a degree due to its high lipophilicity and high levels of non-specific binding. The evidence that PK11195 changes the biophysical properties of lipid bilayers has implications for the functional effects of PK11195 observed at high concentrations. It is possible that some of the TSPO-independent effects of PK11195 could be mediated by PK11195 inserting into the membrane and changing its fluidity to modulate the function of other proteins. A better understanding of the interaction of PK11195 with lipid membranes will lead to a more complete picture of how this ligand exerts its TSPO-independent effects, and how it might influence membrane proteins, including TSPO, by altering the surrounding membrane environment.

In addition, we demonstrated the successful formation of a solid supported TSPO/lipid bilayer with QCM-D, and the detection of ligand interaction with the TSPO. Exposure of the TSPO/lipid bilayer to PK11195 resulted in a larger than expected response, which is likely to indicate a conformational change of the TSPO. This work demonstrates a TSPO-lipid system that can be used for investigating the interaction between TSPO and other ligands and antibodies with QCM-D, with the potential to detect conformational changes. Our neutron reflectometry measurements revealed the thickness and surface coverage of immobilised TSPO in detergent, but the system needs further development to study a TSPO/lipid bilayer and its ligand interactions. The eventual aim of the neutron reflectometry experiments was to explore the conformational changes that were indicated in QCM-D data during interaction with PK11195. Future experiments will aim to improve the stability of the immobilised TSPO layer, such that lipid can be reconstituted around it and ligand interactions can be studied.

There is increasing recognition that drug–membrane interactions may mediate a range of drug responses, possibly by altering biophysical properties of the membrane that affect the conformation and activity of associated membrane proteins. Drug–membrane interactions thus have wider implications for the apparent affinity of drug ligands for their receptors.

In the case of TSPO and its ligands, recent discussions have highlighted variability in binding profiles and affinities between patients, tissues, cell types, and species [68–71]. Some of these apparent affinity variations may not be solely due to sequence variations in the binding domain. A drug–membrane interaction, such as PK11195 with the cell membrane, may contribute to the variable affinities and binding profiles of TSPO ligands, potentially by altering the membrane environment or conformation of the protein, causing homo- or hetero-oligomer formation, or a combination of these. This may, for example, cause the appearance of cooperative binding. Different tissue specific affinities [69] may potentially reflect different molecular environments. For example, different lipid membrane compositions may interact differently with a ligand, notably if it is highly lipophilic, as is the case for most current TSPO ligands, causing apparent differences in the affinity of a ligand for a particular protein target.

The apparent binding affinity of a ligand may thus represent an integration of receptor–ligand and membrane–ligand interactions. Hence, both drug–receptor and drug–membrane interactions should be

considered for a more complete picture of the overall response to a drug. In the case of TSPO it will help us to understand not only how ligands interact directly with TSPO to modulate function, but also how its ligands, such as PK11195, interact with the membrane to modulate the activity of both TSPO and other proteins. A deeper understanding of dual receptor and membrane interactions of a ligand could provide multiple strategies for therapeutic interventions.

Acknowledgements

The authors wish to thank Marie Gillon and Anthony Duff for assistance with protein production (National Deuteration Facility, Bragg Institute, ANSTO), Arwel Hughes (ISIS) for technical support on SURF, Andrew Nelson (Bragg Institute, ANSTO) for support with Motofit, and Frank Heinrich (NIST Nanofab Facility) for gold coated wafers. The authors wish to thank the Bragg Institute, ANSTO for beamtime on the Platypus reflectometer (proposal number 704), ISIS for beamtime on the SURF reflectometer (experiment number RB1120274), and AINSE for travel support for neutron experiments. C.H. was supported by an Australian Postgraduate Award.

Appendix A. Supplementary data

Supplementary data to this article can be found online at http://dx.doi.org/10.1016/j.bbamem.2013.12.013.

References

[1] M. Gavish, I. Bachman, R. Shoukrun, Y. Katz, L. Veenman, G. Weisinger, A. Weizman, Enigma of the peripheral benzodiazepine receptor, Pharmacol. Rev. 51 (1999) 629–650.
[2] L. Veenman, V. Papadopoulos, M. Gavish, Channel-like functions of the 18-kDa translocator protein (TSPO): regulation of apoptosis and steroidogenesis as part of the host-defense response, Curr. Pharm. Des. 13 (2007) 2385–2405.
[3] R. Rupprecht, V. Papadopoulos, G. Rammes, T.C. Baghai, J. Fan, N. Akula, G. Groyer, D. Adams, M. Schumacher, Translocator protein (18 kDa) (TSPO) as a therapeutic target for neurological and psychiatric disorders, Nat. Rev. Drug Discov. 9 (2010) 971–988.
[4] J.K. Ryu, H.B. Choi, J.G. McLarnon, Peripheral benzodiazepine receptor ligand PK11195 reduces microglial activation and neuronal death in quinolinic acid-injected rat striatum, Neurobiol. Dis. 20 (2005) 550–561.
[5] H. Wilms, J. Claasen, C. Rohl, J. Sievers, G. Deuschl, R. Lucius, Involvement of benzodiazepine receptors in neuroinflammatory and neurodegenerative diseases: evidence from activated microglial cells in vitro, Neurobiol. Dis. 14 (2003) 417–424.
[6] R.B. Banati, J. Newcombe, R.N. Gunn, A. Cagnin, F. Turkheimer, F. Heppner, G. Price, F. Wegner, G. Giovannoni, D.H. Miller, G.D. Perkin, T. Smith, A.K. Hewson, G. Bydder, G.W. Kreutzberg, T. Jones, M.L. Cuzner, R. Myers, The peripheral benzodiazepine binding site in the brain in multiple sclerosis: quantitative *in vivo* imaging of microglia as a measure of disease activity, Brain 123 (Pt 11) (2000) 2321–2337.
[7] J.R. Buck, E.T. McKinley, M.R. Hight, A. Fu, D. Tang, R.A. Smith, M.N. Tantawy, T.E. Peterson, D. Colvin, M.S. Ansari, R.M. Baldwin, P. Zhao, S. Guleryuz, H.C. Manning, Quantitative, preclinical PET of translocator protein expression in glioma using 18 -F-N-fluoroacetyl-N-(2,5-dimethoxybenzyl)-2-phenoxyaniline, J. Nucl. Med. 52 (2011) 107–114.
[8] S. Murail, J.C. Robert, Y.M. Coic, J.M. Neumann, M.A. Ostuni, Z.X. Yao, V. Papadopoulos, N. Jamin, J.J. Lacapere, Secondary and tertiary structures of the transmembrane domains of the translocator protein TSPO determined by NMR. Stabilization of the TSPO tertiary fold upon ligand binding, Biochim. Biophys. Acta 1778 (2008) 1375–1381.
[9] N. Jamin, J.M. Neumann, M.A. Ostuni, T.K. Vu, Z.X. Yao, S. Murail, J.C. Robert, C. Giatzakis, V. Papadopoulos, J.J. Lacapere, Characterization of the cholesterol recognition amino acid consensus sequence of the peripheral-type benzodiazepine receptor, Mol. Endocrinol. 19 (2005) 588–594.
[10] E. Joseph-Liauzun, P. Delmas, D. Shire, P. Ferrara, Topological analysis of the peripheral benzodiazepine receptor in yeast mitochondrial membranes supports a five-transmembrane structure, J. Biol. Chem. 273 (1998) 2146–2152.
[11] J.M. Bernassau, J.L. Reversat, P. Ferrara, D. Caput, G. Lefur, A 3D model of the peripheral benzodiazepine receptor and its implication in intra mitochondrial cholesterol transport, J. Mol. Graphics 11 (1993) 236–244(235).
[12] J.K. Seydel, E.A. Coats, H.P. Cordes, M. Wiese, Drug membrane interaction and the importance for drug transport, distribution, accumulation, efficacy and resistance, Arch. Pharm. 327 (1994) 601–610.
[13] M. Lucio, J.L. Lima, S. Reis, Drug–membrane interactions: significance for medicinal chemistry, Curr. Med. Chem. 17 (2010) 1795–1809.
[14] R.A. Gonzalez-Polo, G. Carvalho, T. Braun, D. Decaudin, C. Fabre, N. Larochette, J.L. Perfettini, M. Djavaheri-Mergny, I. Youlyouz-Marfak, P. Codogno, M. Raphael, J. Feuillard, G. Kroemer, PK11195 potently sensitizes to apoptosis induction independently from the peripheral benzodiazepin receptor, Oncogene 24 (2005) 7503–7513.
[15] D. Kletsas, W. Li, Z. Han, V. Papadopoulos, Peripheral-type benzodiazepine receptor (PBR) and PBR drug ligands in fibroblast and fibrosarcoma cell proliferation: role of ERK, c-Jun and ligand-activated PBR-independent pathways, Biochem. Pharmacol. 67 (2004) 1927–1932.
[16] R.B. Walter, J.L. Pirga, M.R. Cronk, S. Mayer, F.R. Appelbaum, D.E. Banker, PK11195, a peripheral benzodiazepine receptor (pBR) ligand, broadly blocks drug efflux to chemosensitize leukemia and myeloma cells by a pBR-independent, direct transporter-modulating mechanism, Blood 106 (2005) 3584–3593.
[17] R.B. Walter, B.W. Raden, M.R. Cronk, I.D. Bernstein, F.R. Appelbaum, D.E. Banker, The peripheral benzodiazepine receptor ligand PK11195 overcomes different resistance mechanisms to sensitize AML cells to gemtuzumab ozogamicin, Blood 103 (2004) 4276–4284.
[18] L. Miccoli, S. Oudard, A. Beurdeley-Thomas, B. Dutrillaux, M.F. Poupon, Effect of 1-(2-chlorophenyl)-N-methyl-N-(1-methylpropyl)-3-isoquinoline carboxamide (PK11195), a specific ligand of the peripheral benzodiazepine receptor, on the lipid fluidity of mitochondria in human glioma cells, Biochem. Pharmacol. 58 (1999) 715–721.
[19] S. Drori, G.D. Eytan, Y.G. Assaraf, Potentiation of anticancer-drug cytotoxicity by multidrug-resistance chemosensitizers involves alterations in membrane fluidity leading to increased membrane permeability, Eur. J. Biochem. 228 (1995) 1020–1029.
[20] L. Yeruva, J.A. Elegbede, S.W. Carper, Methyl jasmonate decreases membrane fluidity and induces apoptosis through tumor necrosis factor receptor 1 in breast cancer cells, Anti-Cancer Drugs 19 (2008) 766–776.
[21] M. Furusawa, H. Tsuchiya, M. Nagayama, T. Tanaka, M. Oyama, T. Ito, M. Iinuma, H. Takeuchi, Cell growth inhibition by membrane-active components in brownish scale of onion, J. Health Sci. 52 (2006) 578–584.
[22] H. Tsuchiya, M. Nagayama, Garlic allyl derivatives interact with membrane lipids to modify the membrane fluidity, J. Biomed. Sci. 15 (2008) 653–660.
[23] F. Giess, M.G. Friedrich, J. Heberle, R.L. Naumann, W. Knoll, The protein-tethered lipid bilayer: a novel mimic of the biological membrane, Biophys. J. 87 (2004) 3213–3220.
[24] S.A. Holt, A.P. Le Brun, C.F. Majkrzak, D.J. McGillivray, F. Heinrich, M. Losche, J.H. Lakey, An ion-channel-containing model membrane: structural determination by magnetic contrast neutron reflectometry, Soft Matter 5 (2009) 2576–2586.
[25] A.P. Le Brun, T.A. Darwish, M. James, Studies of biomimetic cellular membranes using neutron reflection, J. Chem. Biol. Interfaces 1 (2013) 3–24.
[26] K. Ataka, F. Giess, W. Knoll, R. Naumann, S. Haber-Pohlmeier, B. Richter, J. Heberle, Oriented attachment and membrane reconstitution of His-tagged cytochrome c oxidase to a gold electrode: *in situ* monitoring by surface-enhanced infrared absorption spectroscopy, J. Am. Chem. Soc. 126 (2004) 16199–16206.
[27] K.S. Carmon, R.E. Baltus, L.A. Luck, A piezoelectric quartz crystal biosensor: the use of two single cysteine mutants of the periplasmic *Escherichia coli* glucose/galactose receptor as target proteins for the detection of glucose, Biochemistry 43 (2004) 14249–14256.
[28] K.S. Carmon, R.E. Baltus, L.A. Luck, A biosensor for estrogenic substances using the quartz crystal microbalance, Anal. Biochem. 345 (2005) 277–283.
[29] R.E. Baltus, K.S. Carmon, L.A. Luck, Quartz crystal microbalance (QCM) with immobilized protein receptors: comparison of response to ligand binding for direct protein immobilization and protein attachment via disulfide linker, Langmuir 23 (2007) 3880–3885.
[30] J.J. Lacapere, F. Delavoie, H. Li, G. Peranzi, J. Maccario, V. Papadopoulos, B. Vidic, Structural and functional study of reconstituted peripheral benzodiazepine receptor, Biochem. Biophys. Res. Commun. 284 (2001) 536–541.
[31] D. Teboul, S. Beaufils, J.C. Taveau, S. Iatmanen-Harbi, A. Renault, C. Venien-Bryan, V. Vie, J.J. Lacapere, Mouse TSPO in a lipid environment interacting with a functionalized monolayer, Biochim. Biophys. Acta 1818 (2012) 2791–2800.
[32] A.P. Middelberg, B.K. O'Neill, L.B. ID, M.A. Snoswell, A novel technique for the measurement of disruption in high-pressure homogenization: studies on *E. coli* containing recombinant inclusion bodies, Biotechnol. Bioeng. 38 (1991) 363–370.
[33] C.A. Keller, B. Kasemo, Surface specific kinetics of lipid vesicle adsorption measured with a quartz crystal microbalance, Biophys. J. 75 (1998) 1397–1402.
[34] H.M. McConnell, T.H. Watts, R.M. Weis, A.A. Brian, Supported planar membranes in studies of cell–cell recognition in the immune system, Biochim. Biophys. Acta 864 (1986) 95–106.
[35] H.P. Vacklin, F. Tiberg, R.K. Thomas, Formation of supported phospholipid bilayers via co-adsorption with beta-D-dodecyl maltoside, Biochim. Biophys. Acta 1668 (2005) 17–24.
[36] G. Sauerbrey, Verwendung von Schwingquarzen zur Wägung dünner Schichten und zur Mikrowägung, Z. Phys. 155 (1959) 206–222.
[37] H.P. Wacklin, R.K. Thomas, Spontaneous formation of asymmetric lipid bilayers by adsorption of vesicles, Langmuir 23 (2007) 7644–7651.
[38] M. James, A. Nelson, A. Brule, J.C. Schulz, Platypus: a time-of-flight neutron reflectometer at Australia's new research reactor, J. Neutron Res. 14 (2006) 91–108.
[39] M. James, A. Nelson, S.A. Holt, T. Saerbeck, W.A. Hamilton, F. Klose, The multipurpose time-of-flight neutron reflectometer "Platypus" at Australia's OPAL reactor, Nucl. Instrum. Meth. A 632 (2011) 112–123.
[40] A. Nelson, Co-refinement of multiple-contrast neutron/X-ray reflectivity data using MOTOFIT, J. Appl. Crystallogr. 39 (2006) 273–276.
[41] K. Hill, C.B. Pénzes, B.G. Vértessy, Z. Szabadka, V. Grolmusz, É. Kiss, Amphiphilic nature of new antitubercular drug candidates and their interaction with lipid monolayer, in: Z. Hórvölgyi, É. Kiss (Eds.), Colloids for Nano- and Biotechnology, vol. 135, Springer, Berlin Heidelberg, 2008, pp. 87–92.
[42] H. Brockman, Lipid monolayers: why use half a membrane to characterize protein–membrane interactions? Curr. Opin. Struct. Biol. 9 (1999) 438–443.

[43] V. Janout, S. Turkyilmaz, M. Wang, Y. Wang, Y. Manaka, S.L. Regen, An upside down view of cholesterol's condensing effect: does surface occupancy play a role? Langmuir 26 (2010) 5316–5318.
[44] M.K. Ratajczak, Y.T. Ko, Y. Lange, T.L. Steck, K.Y. Lee, Cholesterol displacement from membrane phospholipids by hexadecanol, Biophys. J. 93 (2007) 2038–2047.
[45] M.G. Sarpietro, F. Rocco, D. Micieli, S. Ottimo, M. Ceruti, F. Castelli, Interaction of acyclovir and its squalenoyl-acyclovir prodrug with DMPC in monolayers at the air/water interface, Int. J. Pharm. 395 (2010) 167–173.
[46] A. Ge, H. Wu, T.A. Darwish, M. James, M. Osawa, S. Ye, Structure and lateral interaction in mixed monolayers of dioctadecyldimethylammonium chloride (DOAC) and stearyl alcohol, Langmuir 29 (2013) 5407–5417.
[47] D.I. Fernandez, A.P. Le Brun, T.C. Whitwell, M.A. Sani, M. James, F. Separovic, The antimicrobial peptide aurein 1.2 disrupts model membranes via the carpet mechanism, Phys. Chem. Chem. Phys. 14 (2012) 15739–15751.
[48] K.C. Weng, J.L. Kanter, W.H. Robinson, C.W. Frank, Fluid supported lipid bilayers containing monosialoganglioside GM1: a QCM-D and FRAP study, Colloids Surf. B 50 (2006) 76–84.
[49] G. M'Baye, Y. Mely, G. Duportail, A.S. Klymchenko, Liquid ordered and gel phases of lipid bilayers: fluorescent probes reveal close fluidity but different hydration, Biophys. J. 95 (2008) 1217–1225.
[50] C. Ho, S.J. Slater, C.D. Stubbs, Hydration and order in lipid bilayers, Biochemistry 34 (1995) 6188–6195.
[51] M. Edvardsson, S. Svedhem, G. Wang, R. Richter, M. Rodahl, B. Kasemo, QCM-D and reflectometry instrument: applications to supported lipid structures and their biomolecular interactions, Anal. Chem. 81 (2009) 349–361.
[52] T. Parasassi, M. Di Stefano, M. Loiero, G. Ravagnan, E. Gratton, Cholesterol modifies water concentration and dynamics in phospholipid bilayers: a fluorescence study using Laurdan probe, Biophys. J. 66 (1994) 763–768.
[53] M.P. Boland, C.R. Hatty, F. Separovic, A.F. Hill, D.J. Tew, K.J. Barnham, C.L. Haigh, M. James, C.L. Masters, S.J. Collins, Anionic phospholipid interactions of the prion protein N terminus are minimally perturbing and not driven solely by the octapeptide repeat domain, J. Biol. Chem. 285 (2010) 32282–32292.
[54] G.A. McCubbin, S. Praporski, S. Piantavigna, D. Knappe, R. Hoffmann, J.H. Bowie, F. Separovic, L.L. Martin, QCM-D fingerprinting of membrane-active peptides, Eur. Biophys. J. 40 (2011) 437–446.
[55] A. Mechler, S. Praporski, K. Atmuri, M. Boland, F. Separovic, L.L. Martin, Specific and selective peptide-membrane interactions revealed using quartz crystal microbalance, Biophys. J. 93 (2007) 3907–3916.
[56] R. Richter, A. Mukhopadhyay, A. Brisson, Pathways of lipid vesicle deposition on solid surfaces: a combined QCM-D and AFM study, Biophys. J. 85 (2003) 3035–3047.
[57] K. Kannisto, L. Murtomaki, T. Viitala, An impedance QCM study on the partitioning of bioactive compounds in supported phospholipid bilayers, Colloids Surf. B 86 (2011) 298–304.
[58] J.F. Nagle, S. Tristram-Nagle, Structure of lipid bilayers, Biochim. Biophys. Acta 1469 (2000) 159–195.
[59] Molinspiration, www.molinspiration.com(accessed 2013).
[60] H.P. Vacklin, F. Tiberg, G. Fragneto, R.K. Thomas, Composition of supported model membranes determined by neutron reflection, Langmuir 21 (2005) 2827–2837.
[61] I.P. Sugar, G. Monticelli, Landau theory of two-component phospholipid bilayers. I. Phosphatidylcholine/phosphatidylethanolamine mixtures, Biophys. Chem. 18 (1983) 281–289.
[62] C.A. Helm, P. Tippmann-Krayer, H. Mohwald, J. Als-Nielsen, K. Kjaer, Phases of phosphatidyl ethanolamine monolayers studied by synchrotron X-ray scattering, Biophys. J. 60 (1991) 1457–1476.
[63] S.J. Johnson, T.M. Bayerl, D.C. McDermott, G.W. Adam, A.R. Rennie, R.K. Thomas, E. Sackmann, Structure of an adsorbed dimyristoylphosphatidylcholine bilayer measured with specular reflection of neutrons, Biophys. J. 59 (1991) 289–294.
[64] E. Drolle, N. Kucerka, M.I. Hoopes, Y. Choi, J. Katsaras, M. Karttunen, Z. Leonenko, Effect of melatonin and cholesterol on the structure of DOPC and DPPC membranes, Biochim. Biophys. Acta 1828 (2013) 2247–2254.
[65] V.M. Korkhov, C. Sachse, J.M. Short, C.G. Tate, Three-dimensional structure of TspO by electron cryomicroscopy of helical crystals, Structure 18 (2010) 677–687.
[66] F. Hook, B. Kasemo, T. Nylander, C. Fant, K. Sott, H. Elwing, Variations in coupled water, viscoelastic properties, and film thickness of a Mefp-1 protein film during adsorption and cross-linking: a quartz crystal microbalance with dissipation monitoring, ellipsometry, and surface plasmon resonance study, Anal. Chem. 73 (2001) 5796–5804.
[67] J.J. Lacapere, V. Papadopoulos, Peripheral-type benzodiazepine receptor: structure and function of a cholesterol-binding protein in steroid and bile acid biosynthesis, Steroids 68 (2003) 569–585.
[68] D.R. Owen, O.W. Howell, S.P. Tang, L.A. Wells, I. Bennacef, M. Bergstrom, R.N. Gunn, E.A. Rabiner, M.R. Wilkins, R. Reynolds, P.M. Matthews, C.A. Parker, Two binding sites for [3H]PBR28 in human brain: implications for TSPO PET imaging of neuroinflammation, J. Cereb. Blood Flow Metab. 30 (2010) 1608–1618.
[69] A.M. Scarf, K.M. Auman, M. Kassiou, Is there any correlation between binding and functional effects at the translocator protein (TSPO) (18 kDa)? Curr. Mol. Med. 12 (2012) 387–397.
[70] A.M. Scarf, M. Kassiou, The translocator protein, J. Nucl. Med. 52 (2011) 677–680.
[71] A.M. Scarf, C. Luus, E. Da Pozzo, S. Selleri, C. Guarino, C. Martini, L.M. Ittner, M. Kassiou, Evidence for complex binding profiles and species differences at the translocator protein (TSPO) (18 kDa), Curr. Mol. Med. 12 (2012) 488–493.